ESTIMATING FIRE TEMPERATURE WITH SHORT-WAVE INFRARED BANDS OF HIGH RESOLUTION SATELLITES

Soo Chin Liew

Centre for Remote Imaging, Sensing and Processing (CRISP), National University of Singapore,
Blk S17 Level 2, 10 Lower Kent Ridge Road, Singapore 119076, Singapore,
Email: scliew@nus.edu.sg

KEY WORDS: Fire, Modeling, Thermal imaging, Basis functions, Sentinel-2

ABSTRACT This paper describes a novel technique of detecting daytime fires and estimating fire temperature and fire fractional area using the short-wave infrared (SWIR) bands of high resolution satellites such as Sentinel-2, Landsat-9 and WorldView-3. It is a great challenge to detect daytime fires due to the influence of solar reflected radiance. In our algorithm, the surface reflectance is modeled by a linear combination of a small number of reflectance basis functions. The algorithm could then retrieve the sub-pixel fire temperature, fire area, together with the surface reflectance of the background. This technique would enable detection and characterization of small fires in the tropics, where fires are typically small and not as intense as those in the temperate region.

1. INTRODUCTION

Biomass burning and the associated smoke haze pollution has been a recurring environmental problem in the Southeast Asia region (Miettinen et al. 2013). Fires have been a traditional tool for land clearing by shifting cultivators and small holders. However, the problem becomes more severe with the largescale conversion of land use associated with commercial plantation activities (Koh et al. 2011; Miettinen, Shi and Liew 2012, 2017). During extreme drought periods, fires run out of control resulting in prolonged transboundary smoke haze pollution (Eck et al. 2019; Miettinen et al. 2013). Besides contributing to global warming by the carbon dioxide emission, the smoke haze contains pollutants such as fine aerosol particles, NOX, ozone and volatile organic compounds which have detrimental effects on human health. In the insular Southeast Asia region, fires predominantly occur in the carbon-rich peatlands. For example, during the 2015 fire event, 53% of all fire hotspots detected by Moderate Resolution Imaging Spectroradiometer (MODIS) in Sumatra, Peninsular Malaysia and Borneo resided on peatlands that cover only 12% of this region (Miettinen, Shi and Liew 2017). In the two decades from 1990 to 2010, the proportion of forest cover in the peatlands of the same region fell from 77% to 36%, representing a deforestation rate of 4.9% per year and the land cover change was found to be strongly associated with fire activity (Miettinen, Shi and Liew 2012).

Satellite sensors for detection of hot targets such as forest fires typically operate in the medium to long wave (about 3 to 12 μm) spectral bands. However, currently operating satellites with sensors in this thermal infrared region are limited in their spatial resolutions, ranging from 100 m (Landsat-8), 300 m (VIIRS on Suomi-NPP), to 1 km or more (e.g. MODIS on Terra, Aqua and AHI on Himawari-8). The coarse spatial resolution of the thermal bands results in non-detection of small sub-pixel fires. High resolution satellites such as Landsat-8, Sentinel-2, WorldView-3 and the older SPOT-4, 5 have several short-wave infrared (SWIR) bands which can potentially be used for detection of small fires.

SWIR bands have been employed for estimating fire temperature and fire radiative power using the VIIRS instrument, but only during nighttime (Elvidge et al. 2013; Fisher and Wooster 2018). Attempts to use SWIR bands for daytime fire detection have been reported (Fraser and Landry 2000; Abuelgasim and Fraser 2002). SWIR signals from the SPOT VEGETATION (VGT) sensor was analyzed for detecting fires in boreal forest. It was concluded that the VGT 1.65 μm SWIR band could detect thermal emissions from intense fires, although it was considerably less sensitive to hotspots than the 3.7 μm channel of NOAA-AVHRR (Fraser and Landry 2000). The SWIR band of SPOT4 satellite images have been used for fire detection by visual inspection. Small fires could be detected due to their elevated signals in the SWIR band, in comparison to the visible and NIR bands. These fires would be missed if only visible-NIR bands were used (Lim et al. 2000).

The main difficulty of using SWIR bands in detecting sub-pixel fires during daytime is the influence of the solar reflectance signal. Our previous studies show that sub-pixel fires as small as those occupying 5% of the pixel area can be distinguished from the background pixels in the presence of solar reflected radiance (Liew and Kwoh 2015). However, in order to estimate the fire temperature and fire fractional area, it is necessary to partition the detected

radiance into the solar reflection and thermal emission components. This is a big challenge since the solar component is often similar in magnitude or greater than the thermal component, and the surface reflectance is not a-priori known.

In this paper, we develop a theoretical model for the detection of fires using SWIR bands and design a novel algorithm for estimating the sub-pixel fire temperature and area. We employ a set of basis functions to represent the spectral reflectance of a multispectral sensor from the visible to the SWIR bands. As an example, we construct an orthonormal set of basis functions using reflectance measurements extracted from the NASA's JPL ECOSTRESS spectral library and aggregated to the Sentinel-2 spectral bands. We found that four basis components are sufficient to reconstruct the reflectance spectra from the spectral library with good accuracy. By fitting the radiance spectra measured by the Sentinel-2 sensor from the visible to SWIR bands, the surface reflectance, fire temperature and fire area can be derived. This algorithm has been tested on a Sentinel-2 image of a test area in Central Kalimantan during the fire session in 2019. The capability to detect small fires and estimating the fire temperature will enable better fire management before they become severe and spread uncontrollably resulting in transbouundary haze pollution and ecological disaster. Information about the fire radiative power is useful for modeling the gaseous and particulates emission for climate studies.
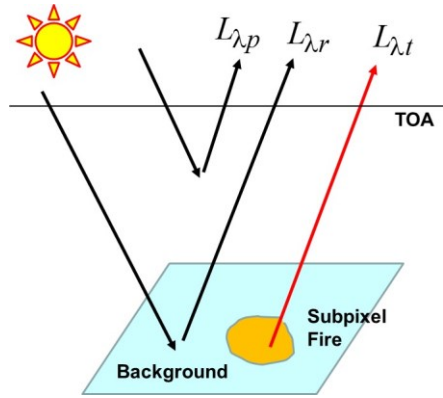
2. THEORETICAL MODEL

Figure 1. Components of the radiance detected at the top of the atmosphere from a sub-pixel fire

In a simplified model of fire detection in the SWIR region, the radiance detected at the top of the atmosphere (TOA) can be modeled by the sum of three components: 1) Atmospheric path radiance $L_{\lambda p}$ due to scattering of sunlight by the atmosphere; 2) Reflected radiance $L_{\lambda r}$ due to reflection of solar irradiance by the ground; 3) Thermal radiance $L_{\lambda t}$ due to thermal emission from the ground surface (Figure 1). The ground target is a sub-pixel fire that occupies a fraction f of the pixel area with a fire temperature T_f while the unburned background has a temperature T_b. The spectral reflectance of the background surface is $\rho(\lambda)$ while the fire is assumed to be a perfect blackbody. The solar irradiance at TOA is E_λ. The reflected radiance and thermal radiance at TOA are,

$$L_{\lambda r} = t^\downarrow(\lambda) t^\uparrow(\lambda) \rho(\lambda) E_\lambda / \pi \tag{1}$$

$$L_{\lambda t} = t^\uparrow(\lambda) \left[f B_\lambda(T_f) + (1-f)(1-\rho(\lambda)) B_\lambda(T_b) \right] \tag{2}$$

The function $B_\lambda(T)$ is Planck's blackbody radiance at temperature T. The two transmittance functions $t^\downarrow(\lambda)$ and $t^\uparrow(\lambda)$ are, respectively, the downward and upward transmittance of the atmosphere, which depends on the solar angle, view angle and the atmospheric conditions. The transmittance functions together with the atmospheric path radiance can be calculated using a radiative transfer code such as 6SV and Modtran. It can be shown that the thermal emission from the unburned background surface is negligible compared to the emission from the fire. Hence, the TOA radiance can be expressed as,

$$L_\lambda = t^\downarrow(\lambda) t^\uparrow(\lambda) \rho(\lambda) E_\lambda / \pi + t^\uparrow(\lambda) f B_\lambda(T_f) + L_{\lambda p} \tag{3}$$

The unknown parameters in this equation (3) are the fire temperature T_f, the fire fractional area f and the reflectance $\rho(\lambda)$ of the background surface. Suppose that the TOA radiance is measured at N wavelengths $\lambda = \lambda_j \ (j = 1, 2, ..., N)$. Hence, we can form N equations to solve for N + 2 unknowns. This is thus an

under-determined problem which has no unique solutions.

In order to solve the equation (3), we can express the reflectance in terms of a series of $M \leq N$ orthonormal basis functions $r_i(\lambda_j)$ in the form,

$$\rho(\lambda_j) = \sum_{i=1}^{M} a_i r_i(\lambda_j) \quad (j = 1, 2, ..., N) \tag{4}$$

where a_i is the coefficient for the i-th basis function. Hence, the number of unknowns is reduced to $M+2$. If $M + 2 < N$, the equation (3) becomes over-determined (i.e. the number of equations N is greater than the number of unknowns M+2) and can be solved by using an optimization procedure that seeks a solution minimizing the RMS error between the measured and the model TOA radiance,

$$\varepsilon_{rms} = \sqrt{\frac{1}{N} \sum_{j=1}^{N} (L_j - \hat{L}_j)^2} \tag{5}$$

where L_j is the TOA radiance measured at the jth-spectral band and $\hat{L}_j$ is the model radiance computed using equations (3) and (4).

3. METHODS

As a demonstration of retrieving fire temperature from SWIR data, we developed the retrieval mode for the spectral bands of the Sentinel-2 MultiSpectral Instrument (MSI) (Table 1). Sentinel-2 MSI has 13 spectral bands, with 2 in the SWIR region. Only ten spectral bands with 10 m or 20 m resolution were used, i.e. all except Bands 1, 9 and 10.

Table 1. Spectral bands of Sentinel-2 MSI

Band number	Spatial Sample Distance (m)	Central wavelength (nm)	Bandwidth (nm)	Lmin	Lref	Lmax	SNR (at Lref)	Noise Equivalent Radiance (W.m^{-2}.sr^{-1}.µm^{-1})
1	60	443	20	16	129	588	129	1.000
2	10	490	65	11.5	128	615.5	154	0.831
3	10	560	35	6.5	128	559	168	0.762
4	10	665	30	3.5	108	484	142	0.761
5	20	705	15	2.5	74.5	449.5	117	0.637
6	20	740	15	2	68	413	89	0.764
7	20	783	20	1.5	67	387	105	0.638
8	10	842	115	1	103	308	174	0.592
8A	20	865	20	1	52.5	308	72	0.729
9	60	945	20	0.5	9	233	114	0.079
10	60	1 375	30	0.05	6	45	50	0.120
11	20	1 610	90	0.5	4	70	100	0.040
12	20	2 190	180	0.1	1.5	24.5	100	0.015

The reflectance basis functions were constructed using the reflectance spectra from NASA JPL ECOSTRESS Spectral Library (Meerdink et al. 2019). The spectral library contains over 2000 reflectance samples organized in 3 main categories: Manmade, Soil, Vegetation. The Vegetation category is further divided into Trees, Shrubs and Grass. One hundred reflectance spectra were randomly selected from the spectral library, with 25 spectra in each of the 4 categories (manmade, soil, trees, shrubs). Each spectrum is aggregated to the 10 selected MSI bands using their respective spectral response functions. Ten orthonormal basis functions were constructed using the singular value decomposition (SVD) procedure. It was found that the first 4 basis functions were sufficient to reconstruct all the reflectance to a high degree of accuracy.

One Sentinel-2A scene (Level 1C) covering a fire area in Central Kalimantan on 3 September 2019 was downloaded from USGS Earth Explorer portal. The digital numbers were converted to TOA radiance and resampled to 20 m pixel width (Figure 2). The TOA radiance at selected pixels were extracted to test the temperature retrieval algorithm. The test pixels were located at sites of active fires, recent burn scars and unburned natural vegetation. Retrievals were conducted in Microsoft Excel using the built-in Solver optimization module.
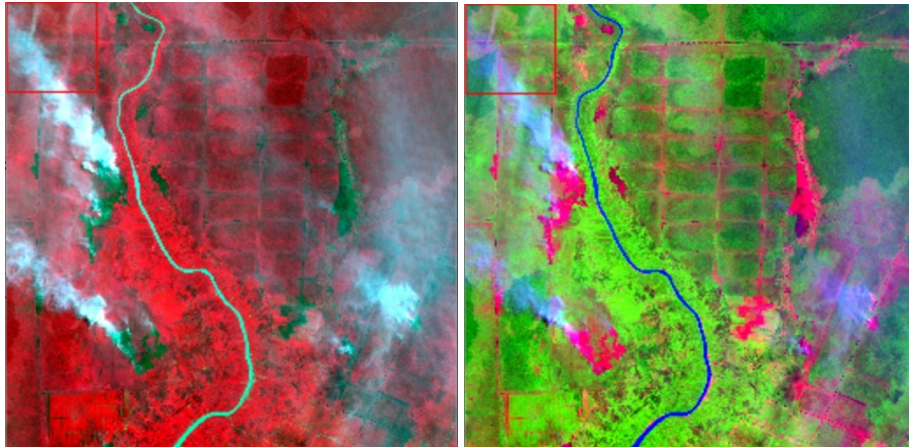
Figure 2. A subscene of a Sentinel-2A image showing smoke plumes of active fires and burn scars.
False color display. Left: RGB = Bands 8,4,3. Right: RGB = Bands 12,8,4.

4. RESULTS AND DISCUSSIONS

As a demonstration of the temperature retrieval model, the results of retrieval at 3 sampling points (Figure 3) will be shown. Sampling point A is located at the site of an active fire, point is at a recent burn scar while point C is unburned natural vegetation.
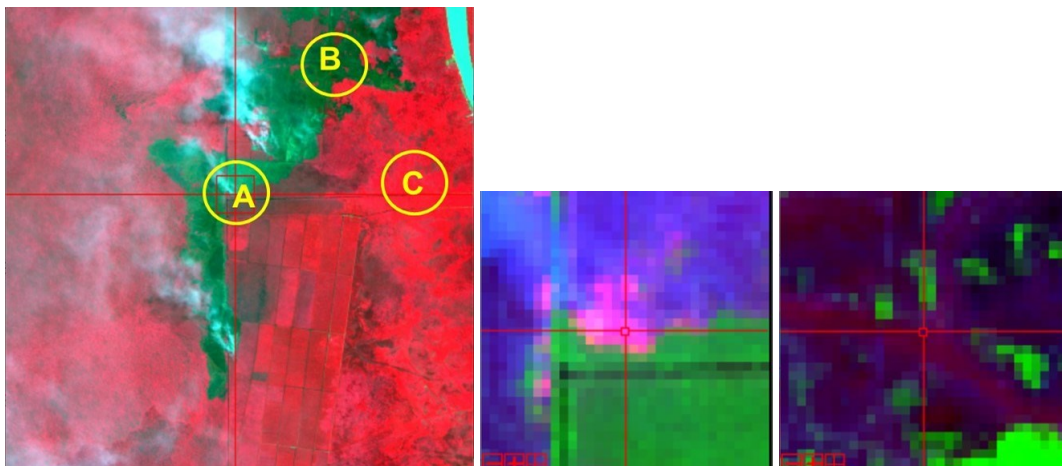

Figure 3. Sapling points for testing of the temperature retrieval model. Left: False color image (RGB = 8,4,3) showing the locations of the 3 points labeled A, B and C. Middle: Zoom-in image (RGB=12,8,4) of Location A, active fire. Right: Zoom-in image (RGB=12,8,4) of Location B, recent burn scar.
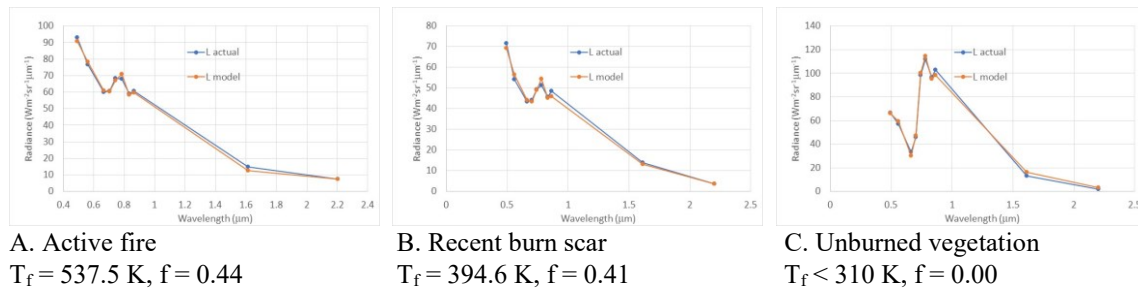

A. Active fire
T_f = 537.5 K, f = 0.44

B. Recent burn scar
T_f = 394.6 K, f = 0.41

C. Unburned vegetation
T_f < 310 K, f = 0.00

Figure 4. Results of temperature retrieval for Points A (Left), B (Middle) and C (Right).The blue lines are the measured TOA radiance while the red lines are the best fit radiance computed using equation 3. The retrieved fire temperature and fire fractional area are shown below the respective graphs.

The results of temperature retrieval at the 3 sampling points are shown in Figure 4. At each location, the measured TOA radiance (blueline) and the best fit model radiance (red line) computed with Equation (3) are plotted at the 10

selected MSI bands. It can be seen that the model (Equation 3) is able to reproduce the measured values very well in all the three cases. For Point A (active fire), the retrieved fire temperature is 537.5 K and the fire fractional area is 0.44. The fire temperature of 537.5 K indicates that it is a smoldering fire and the fire occupies an area of approximately 176 m^2. For Point B (recent burn scar), the retrieved temperature is 394.6 K which is quite high compared to the normal ambient temperature of about 300 K but it is low compared to the fire temperature. Hence, the result is consistent with the interpretation that it is newly burned. For Point C (unburned vegetation), the retrieved temperature is lower than 310 K and the fire fraction is zero. Thus, the retrieval model is able to identify this pixel as a non-fire.

The sensitivity of this temperature retrieval algorithm depends on the radiance detected at the SWIR bands. If the thermal emission of the hot target is lower than the noise equivalent radiance (NEL), this algorithm will not be able to resolve the target temperature. The NEL of Band 12 (2.2 μm) is 0.015 $Wm^{-2}sr^{-1}μm^{-1}$, which is equivalent to a temperature of 310 K. Hence, the detection limit of this model is about 310 K. If the temperature of the target (fire or hot surface) is lower than this limit, it is then not possible to detect the target with this model.

The retrieval procedure of this model is implemented by running an iterative optimization routine. As the iterative process is computationally intensive, it is still not practical to implement it throughout an image with millions of pixels. The next step is to design an optimization procedure that does not involve extensive iterations.

5. CONCLUSIONS

In this paper, we have demonstrated the implementation of a novel algorithm that is capable of daytime retrieving sub-pixel fire temperature using the SWIR bands. The main challenge is to partition the TOA radiance into the reflective and thermal emissive components. We overcome this difficulty by modeling the surface reflectance using a suitably designed set of basis functions. We show that 4 basis functions are sufficient to reconstruct the surface reflectance at 10 spectral bands of Sentinel-2 MSI instrument. Although the results have not yet been validated, the retrieved temperature values seem plausible. This technique would enable the detection of small fires with SWIR bands of high resolution satellites, such as Sentinel-2, Landsat-8 and WorldView-3. The capability would enable better fire management before they become severe and spread uncontrollably.

6. REFERENCES

Abuelgasim, A. and Fraser, R. (2002). Day and night-time active fire detection over North America using NOAA-16 AVHRR data. IEEE International Geoscience and Remote Sensing Symposium 2002, vol. 3, pp. 1489-1491.

Eck, T. F., et al. (2019). AERONET remotely sensed measurements and retrievals of biomass burning aerosol optical properties during the 2015 Indonesian burning season, Journal of Geophysical Research: Atmospheres 124(8), 4722-4740.

Elvidge, C. D., Zhizhin, M., Hsu, F.-C. and Baugh, K. E. (2013). VIIRS nightfire: Satellite pyrometry at night. Remote Sensing 5(9), 4423-4449.

Fisher, D. and Wooster, M. J. (2018). Shortwave IR adaption of the mid-infrared radiance method of fire radiative power (FRP) retrieval for assessing industrial gas flaring output, Remote Sensing 10, 305-327.

Fraser, R. H., Li, Z. and Landry, R. (2000). SPOT VEGETATION for characterizing boreal forest fires. Int. J. Rem. Sens 21(18), 3525-3532.

Koh, L. P., Miettinen, J., Liew, S. C. and Ghazoul, J. (2011). Remotely sensed evidence of tropical peatland conversion to oil palm. PNAS 108(12), 5127-5132.

Liew, S. C. and Kwoh, L. K. (2015). Detecting fires using high resolution multispectral short-wave infrared satellite sensors, Proc. 36th Asian Conference on Remote Sensing (ACRS2015), paper no. Th1.5.5.

Lim, K. H., Kwoh, L. K., Liew, S. C. and Lim, H. (2000), Forest fire monitoring with SPOT-4 satellite uimagery. Proceedings of the 21st Asian Conference on Remote Sensing, 4-8 Dec 2000, Taipei, Taiwan, Vol. 1, 252-257.

Meerdink, S. K., Hook, S. J., Roberts, D. A. and Abbott, E. A. (2019). The ECOSTRESS spectral library version 1.0. Remote Sensing of Environment, 230(111196), 1–8.

Miettinen, J., Shi, C. and Liew, S. C. (2012). 1990 - 2010: Two decades of destruction for Southeast Asian peat swamp forests. Frontiers in Ecology and the Environment 10(3), 124-128

Miettinen, J., et. al. (2013). Detection of vegetation fires and burnt areas by remote sensing in insular Southeast Asian conditions: current status of knowledge and future challenges. International Journal of Remote Sensing 34(12), 4344-4366.

Miettinen, J., Shi, C. and Liew, S. C. (2017). Fire distribution in Peninsular Malaysia, Sumatra and Borneo in 2015 with special emphasis on peatland fires. Environmental Management 60(4), 747-757.